The dynamic properties of a nuclear coactivator binding domain are evolutionarily conserved

Elin Karlsson[1], Frieda A. Sorgenfrei[1,†], Eva Andersson[1], Jakob Dogan[1], Per Jemth[1,*], and Celestine N. Chi[1,2,*]

[1]Department of Medical Biochemistry and Microbiology, Uppsala University, BMC Box 582, SE-75123 Uppsala, Sweden.

[2]Department of Pharmaceutical Biosciences, Uppsala University, BMC Box 582, SE-75123 Uppsala, Sweden

[†]Present address: acib GmbH, Krenngasse 37, 8010 Graz c/o University of Graz, Institute of Chemistry, NAWI Graz, BioTechMed Graz, Heinrichstrasse 28, 8010 Graz, Austria

*Correspondence to

Celestine Chi, Celestine.Chi@imbim.uu.se

Per Jemth, Per.Jemth@imbim.uu.se

ABSTRACT

Evolution of proteins is constrained by their structure and function. While there is a consensus that the plasticity of intrinsically disordered proteins relaxes the structural constraints on evolution there is a paucity of data on the molecular details of these processes. The Nuclear co-activator binding domain (NCBD) from CREB-binding protein is a protein-protein interaction domain, which contains a hydrophobic core but is not behaving as a typical globular domain, and has been desribed as 'molten-globule like'. The highly dynamic properties of NCBD makes it an interesting model system for evolutionary structure-function investigation of intrinsically disordered proteins. We have here compared the structure and biophysical properties of an ancient version of NCBD present in a bilaterian animal ancestor living around 600 million years ago with extant human NCBD. Using a combination of NMR spectroscopy, circular dichroism and kinetic methods we show that although NCBD has increased its thermodynamic stability, it has retained its dynamic biophysical properties in the ligand-free state in the evolutionary lineage leading from the last common bilaterian ancestor to humans. Our findings suggest that the dynamic properties of NCBD have been maintained by purifying selection and thus are important for its function, which includes mediating several distinct protein-protein interactions.

Introduction

Evolution has shaped proteins into a wide spectrum of structure, stability and dynamics, with fully disordered proteins at one end of the scale and well-folded globular proteins at the other one (*1*). It is becoming clear that dynamic properties *per se* are important for protein function (*1–3*) but it is not trivial to prove that the dynamics are essential for biological function and not merely a general property of proteins. The Nuclear Coactivator Binding Domain (NCBD) is a small (approximately 50 residues) domain from CREB-binding protein (CBP, also called CREBBP), which is a transcriptional coactivator with histone acetylase activity and present in all animals (*4*). The NCBD domain has a hydrophobic core, but is very dynamic and even verging on being intrinsically disordered (*5–7*). It has therefore been described as "molten-globule-like" (*8–11*). The fact that NCBD possesses properties of both intrinsically disordered and globular proteins makes it an interesting system for assessing the role of dynamics in protein structure and how it modulates function. We have previously subjected NCBD to "evolutionary biochemistry" (*12*, *13*). Thus, we resurrected and characterized ancestral versions of NCBD and its protein ligand CBP-Interacting Domain (CID) from the NCOA1, 2 and 3 protein family (with three members in human called Src1, Tif2 and ACTR, respectively) to address the evolution of affinity in this protein-protein interaction. The oldest "maximum likelihood" (ML) NCBD variant we could resurrect was present before the Cambrian period, some 540-600 million years ago, in the common ancestor of all present-day animals with bilaterian symmetry. These animals are divided into deuterostomes and protostomes (D/P) and the ancestral NCBD domain is denoted $NCBD_{D/P}^{ML}$. It was shown to bind the CID domain with relatively low affinity ($K_d \sim$ 1-5 μM) whereas more recent variants of NCBD in the vertebrate lineage

64 (ca. 440 million years ago) had acquired present-day affinity for CID (K_d ~ 0.1-0.2 μM).
65 Structural characterization of ancestral and present-day CID/NCBD complexes showed
66 that the increase in affinity observed for more modern NCBD variants was due to a
67 combination of factors. These include several new interactions driving structural and
68 dynamic changes in the complex, such as formation of a third α helix in CID upon
69 interaction (*13*). In the present paper, we investigate the structural and biophysical
70 properties of the ligand-free state of the ancestral Cambrian-like low-affinity
71 $NCBD_{D/P}^{ML}$ and compare it to that of high-affinity present-day $NCBD_{Human}$ to track the
72 evolution of structure and dynamics and their relation to function. The comparison
73 reveals that the overall properties of the ancestral $NCBD_{D/P}^{ML}$ domain are very similar
74 to those of the present-day $NCBD_{Human}$. In general, conservation implies function. Thus,
75 this conservation of a highly dynamic structure and molten-globule like properties
76 suggest that these features are subject to purifying selection and hence that dynamics
77 are indeed important for the biological function of NCBD.
78
79
80 **Results**
81
82 **The structures of ancient $NCBD_{D/P}$ and extant $NCBD_{Human}$ are similar but not**
83 **identical.** Because of its dynamic properties it is challenging to solve the structure of
84 ligand-free NCBD (*8*). First, we performed experiments with ^{15}N labeled $NCBD_{D/P}^{ML}$.
85 We discovered by serendipity that low pH significantly improved the quality of the
86 $^{1}H^{15}N$ heteronuclear single quantum coherence (HSQC) spectrum resulting in well
87 dispersed peaks for $NCBD_{D/P}^{ML}$ (Fig. 1), and allowing for a near complete assignment
88 of the backbone and side-chain residues from NMR 3D experiments using ^{13}C and ^{15}N

89 labeled samples. The NMR structure was thus determined at pH 2.4 by measuring 3D
90 1H-1H $^{13}C/^{15}N$ resolved NOESY experiments for distance restraints determination and
91 $^{3}J_{HNHA}$ for dihedral angle determination. The structure of $NCBD_{D/P}^{ML}$ was found to be
92 overall consistent with that of the free (*8*) and bound $NCBD_{Human}$ (*6*) and bound
93 $NCBD_{D/P}^{ML}$ determined at pH 6.8 (*13*) (Fig. 1). However, a detailed comparison
94 between $NCBD_{D/P}^{ML}$ and $NCBD_{Human}$ shows that the orientation of helix 1 (α1) and
95 helix 3 (α3) differ between the structures. Upon structural alignment of $NCBD_{Human}$
96 and $NCBD_{D/P}^{ML}$, we observed that both the α1 and α3 from $NCBD_{D/P}^{ML}$ are slightly
97 tilted away relative to that of $NCBD_{Human}$. We also observed that for CID-bound
98 $NCBD_{D/P}^{ML}$ and free $NCBD_{D/P}^{ML}$ the α3 displayed structural rearrangements (Fig. 2).
99
100 The amino acid sequence of $NCBD_{D/P}^{ML}$ was reconstructed using phylogenetic
101 methods[4]. The probability is low that the resulting maximum likelihood sequence is
102 identical to the actual sequence present in the ancestor. Thus, $NCBD_{D/P}^{ML}$ is rather one
103 of a large number of likely ancestral variants with similar properties. We wondered if
104 errors in the sequence of $NCBD_{D/P}^{ML}$ resulted in the differences we observe in helix α1
105 and α3 compared to $NCBD_{Human}$. To investigate this further, and to test how structurally
106 robust the dynamic NCBD domain is, we performed a control experiment where we
107 expressed, purified and characterized an alternative $NCBD_{D/P}$ variant denoted
108 $NCBD_{D/P}^{AltAll}$. In this $NCBD_{D/P}^{AltAll}$ variant, all residues with a posterior probability
109 lower than around 0.9 (*12*) were replaced with the second most likely residue at that
110 position. For example, residue 2107 is His with 87% probability and Gln with 12%
111 probability in the ancestral $NCBD_{D/P}$. Thus, $NCBD_{D/P}^{ML}$ has a His in position 2107 and
112 $NCBD_{D/P}^{AltAll}$ a Gln residue. $NCBD_{D/P}^{AltAll}$ can be considered a "worst case scenario"
113 variant and a good control of the robustness of conclusions drawn from resurrection

experiments. If ML and AltAll variants display similar properties it is very likely that the actual ancestral protein shares these properties as well. Because of this, an AltAll variant is a convenient alternative to combinations of point mutations (*14*). $NCBD_{D/P}^{AltAll}$ contains six substitutions as compared to $NCBD_{D/P}^{ML}$ (Fig. 1). Three of the differences between $NCBD_{D/P}^{ML}$ and $NCBD_{D/P}^{AltAll}$ are in the N-terminus, but only one of these is in a structured region, a Gln2065→Pro at the beginning of α1. The other three differences are Ser2078→Asn in the loop between α1 and α2, a solvent exposed Gln2088→His in α2 and His2108→Gln at the C-terminus. We solved the NMR structure of $NCBD_{D/P}^{AltAll}$ (Fig. S1) and found that it folds into a similar structure as the other NCBD domains. The overall RMSD between $NCBD_{D/P}^{AltAll}$ and $NCBD_{D/P}^{ML}$ was 7.9 Å. As a comparison, the overall RMSD between $NCBD_{Human}$ and $NCBD_{D/P}^{AltAll}$ or $NCBD_{D/P}^{ML}$ were 4.5 Å and 7.0 Å, respectively. Detailed inspection of the structures revealed differences in the backbone between $NCBD_{D/P}^{ML}$ and $NCBD_{D/P}^{AltAll}$, especially in the orientations of the helices. An overlay of the structures of $NCBD_{D/P}^{AltAll}$, $NCBD_{D/P}^{ML}$, and $NCBD_{Human,}$ shows differences between α1, α2 and α3 (Fig. S1). One reason for the differences is that there are several long-range NOEs in $NCBD_{D/P}^{AltAll}$ that are not present in $NCBD_{D/P}^{ML}$, between the following pairs of residues: 2068/2082, 2069/2080, 2070/2083 and 2071/2099. There is also an NOE between Ile2062 Hγ, and Pro2065 Hα, two of the substituted residues in $NCBD_{D/P}^{AltAll}$. However, there appears to be a consistency in the hydrophobic core of both $NCBD_{D/P}^{ML}$ and $NCBD_{D/P}^{AltAll}$ since the single Phe residue at position 2100 is packed and buried in a similar fashion in the two variants. Phe2100 is stabilized by Leu2090 in $NCBD_{D/P}^{ML}$, and both Ile2089 and Leu2090 in $NCBD_{D/P}^{AltAll}$ (Fig. 3). Interestingly, this is the same kind of packing that was observed in the free $NCBD_{human}$ domain (*8*), suggesting conserved features in the hydrophobic core.

139

140 Despite the differences discussed in the previous paragraph, the overall biophysical
141 properties of $NCBD_{D/P}^{ML}$ and $NCBD_{D/P}^{AltAll}$ were found to be similar (Fig. S2)
142 corroborating the overall similarity seen with the NMR structures. Specifically, to test
143 the affinity of $NCBD_{D/P}^{AltAll}$ for CID, we expressed and purified ML and AltAll
144 versions of its ligand CID_{1R} based on our previous reconstruction (*8*). K_d values of all
145 four combinations ($NCBD_{D/P}^{ML}$ and $NCBD_{D/P}^{AltAll}$ with CID_{1R}^{ML} and CID_{1R}^{AltAll}) were
146 between 2-9 μM (Fig. S2a), which is in the same range as previous estimates of affinity
147 of the ancestral complex (*12*, *13*). Furthermore, the stability as monitored by urea
148 denaturation (Fig. S2b) and thermal denaturation (Fig. S2c-d) were similar for
149 $NCBD_{D/P}^{ML}$ and $NCBD_{D/P}^{AltAll}$. Thus, based on the highly similar biophysical
150 properties of $NCBD_{D/P}^{ML}$ and $NCBD_{D/P}^{AltAll}$ we conclude that our conclusions are
151 robust with regard to the uncertainty in the reconstructed sequence.

152

153 **Ancient $NCBD_{D/P}$ is less thermodynamically stable than extant $NCBD_{Human}$ but**
154 **display a similar pH dependence with regard to structure and stability.** Since the
155 $NCBD_{D/P}^{ML}$ structure was determined at low pH, we next investigated how pH
156 influences the fold and stability. First, we performed ^{1}H-^{15}N HSQC-monitored pH
157 titrations of $NCBD_{D/P}^{ML}$ and compared them to those of $NCBD_{Human}$ at different pH
158 values (Fig. 4). The NMR titration experiments showed that $NCBD_{D/P}^{ML}$ is as folded at
159 low pH as it is at high pH values. However, the peaks (^{1}H-^{15}N) are much sharper
160 (reduced line-width) at lower pH values indicating less conformational heterogeneity.
161 Second, the CD-monitored urea denaturation experiments showed identical stability
162 pattern at two pH values (3.0 and 7.4) for both ancient $NCBD_{D/P}^{ML}$ and extant
163 $NCBD_{Human}$ (Fig. 4c and d, Supplementary table S1). This indicates that while at lower

164 pH the $NCBD_{D/P}^{ML}$ still exhibits the same stability as at high pH values, there is a shift
165 in conformational heterogeneity towards a single state at low pH. Furthermore, whereas
166 the apparent thermodynamic stability differs by approximately 1 kcal mol^{-1} for ancient
167 $NCBD_{D/P}^{ML}$ and extant $NCBD_{Human}$, both are largely unaffected by a drop in pH to 3.0
168 (Supplementary Table S1). The observed difference in stability between $NCBD_{D/P}^{ML}$
169 and $NCBD_{Human}$ appears to be a robust result. Previous experiments suggested that the
170 ancestral $NCBD_{D/P}^{ML}$ was slightly less stable than younger and extant NCBD variants
171 as judged by urea denaturation experiments at pH 7.5 (*12*). However, the broad
172 unfolding transition of NCBD resulting from its small hydrophobic core leads to a large
173 error in the $m_{D\text{-}N}$ value, which makes it difficult to unequivocally determine the
174 thermodynamic stability of the domain. However, all present results (including
175 experiments on the stabilized $NCBD_{D/P}^{ML}$ variant $NCBD_{D/P}^{T2073W}$ (Supplementary
176 Table S1) agree well with the previous experiments and we can therefore conclude with
177 greater confidence that the ancestral $NCBD_{D/P}^{ML}$ was less thermodynamically stable
178 than evolutionarily younger variants. Interestingly, with some exceptions (*15*, *16*),
179 ancestral reconstructions often yield proteins with higher thermostability, which
180 correlates with thermodynamic stability, than extant proteins, either due to a bias for
181 stability in the reconstruction or due to higher temperatures in past times (*17–21*), like
182 during Cambrian (*22*, *23*). In any case, ancestral NCBD appears to have populated the
183 native state to a lesser extent than present day human NCBD.
184
185 **Ancient $NCBD_{D/P}^{ML}$ and extant $NCBD_{Human}$ display similar temperature-**
186 **dependent structural changes.** Previous experiments demonstrated that $NCBD_{Human}$
187 shows an apparent non-cooperative unfolding behavior when subjected to increasing
188 temperatures, as monitored by CD (*6*, *8*). This behavior may result from a low $\Delta H_{D\text{-}N}$

189 value rather than a true non-cooperative unfolding. (The urea denaturation experiments
190 are consistent with a cooperative two-state unfolding.) We compared ^{1}H-^{15}N HSQC
191 and CD spectra, respectively, of $NCBD_{D/P}^{ML}$ and $NCBD_{Human}$ at different temperatures
192 (Fig. 5). In agreement with the previous data we observed that both variants unfold non-
193 cooperatively with temperature as monitored by the increase in molar ellipticity at 222
194 nm suggesting loss of α-helix as the temperature is increased. However, for both
195 $NCBD_{D/P}^{ML}$ and $NCBD_{Human}$ the signal is not completely lost even at 363 K (90°C)
196 underscoring that this is not a typical native to highly-disordered-denatured state
197 transition. Furthermore, ^{1}H-^{15}N HSQC spectra of $NCBD_{D/P}^{ML}$ at temperatures up to 333
198 K (60°C) show well dispersed peaks indicating a presumably globular, collapsed
199 architecture (Fig. S3) and corroborating the notion that NCBD retains structure at high
200 temperatures.
201
202 **Rate constants for (un)folding of ancient $NCBD_{D/P}^{ML}$ and extant $NCBD_{Human}$.** The
203 folding of human NCBD is complex, and, based on kinetic experiments on a human
204 NCBD variant, we proposed a three-state system involving 'native' NCBD (*i.e.*, the
205 solved structure), an intermediate state with unknown structure and a denatured state,
206 which likely retains significant structure under native conditions (*24*). Rate constants
207 in the same order was determined by relaxation dispersion NMR experiments by
208 Kjaergaard et al. (*10*) It is clear from the NMR experiments that low pH promotes the
209 native state of NCBD and that pH does not affect the thermodynamic stability as
210 monitored by urea denaturation experiments to any significant extent, neither for
211 $NCBD_{D/P}^{ML}$ nor $NCBD_{Human}$. Previous folding experiments on $NCBD_{Human}$ (*24*)
212 involving jumps from low to neutral pH thus resulted in small shifts in the equilibria
213 between the native, intermediate and denatured states yielding the observed kinetic

214 transients. In fact, a likely explanation for the better NMR spectra at low pH is that
215 there is less of the intermediate state under these conditions.
216
217 To further compare the biophysical properties of ancient $NCBD_{D/P}^{ML}$ and extant
218 $NCBD_{Human}$ we performed kinetic folding experiments using stopped-flow as well as
219 temperature-jump fluorescence spectroscopy. To achieve this we introduced a Trp at
220 position 2073 in $NCBD_{D/P}^{ML}$ as previously done in the folding studies of $NCBD_{Human}$
221 (*24*). This modification resulted in a thermodynamic stabilization of around 1 kcal mol^{-}
222 ^{1} for both $NCBD_{D/P}^{T2073W}$ and $NCBD_{Human}^{T2073W}$ (Fig. 6a-b, Supplementary Table S1).
223 Previous folding experiments were performed on a slightly longer $NCBD_{Human}$ variant
224 (residues 2058-2116), which was used in the original studies of CID/NCBD (*6*). In our
225 resurrection studies, we used a shorter version of $NCBD_{Human}$, only containing the
226 evolutionarily conserved region (residues 2062-2109). Therefore, we first repeated the
227 temperature-jump folding experiments for $NCBD_{Human}^{T2073W}$ and showed that the
228 shorter construct used in our evolutionary studies displayed similar kinetics as the
229 longer construct (Fig. 6c). We then performed folding experiments with
230 $NCBD_{D/P}^{T2073W}$. The kinetic transients of $NCBD_{D/P}^{T2073W}$ from temperature jump
231 experiments had lower signal-to-noise than those of $NCBD_{Human}^{T2073W}$, but observed
232 rate constants were in the same range (Fig. 6d). To investigate the folding kinetics
233 further we used stopped-flow fluorimetry, which has a lower time resolution but can be
234 used to compare folding rate constants for $NCBD_{D/P}^{T2073W}$ and $NCBD_{Human}^{T2073W}$ at low
235 temperature (Fig. 6e-f). The stopped-flow folding experiments were conducted by
236 making pH jumps from a 5 mM HCl solution (pH ~ 2) to a buffer solution of 20 mM
237 sodium phosphate (pH 7.4, 150 mM NaCl, 1 M TMAO) and monitoring the relaxation
238 through a 330 nm band-pass filter at 4°C. The low temperature is necessary to reduce

239 the observed rate constant such that the folding or other conformational transitions take
240 place in the millisecond time window. We observed two kinetic phases for
241 $NCBD_{Human}^{T2073W}$ (one fast phase with a negative amplitude and a second slower phase
242 with a positive amplitude) but only one kinetic phase for $NCBD_{D/P}^{T2073W}$ (with a
243 positive amplitude). The values of the observed rate constants for $NCBD_{Human}^{T2073W}$
244 (~300 s^{-1} and ~70 s^{-1}, respectively) were similar to those observed previously for the
245 longer construct (*24*). The single value obtained for the $NCBD_{D/P}^{T2073W}$ was ~140 s^{-1}.
246 Trp fluorescence is a very sensitive but crude structural probe. Thus, the number of
247 kinetic phases in folding experiments could be dependent on small structural
248 rearrangements around the Trp. Nevertheless, the observed rate constant for
249 $NCBD_{D/P}^{T2073W}$ in the stopped flow pH jump experiment is in the same range as the two
250 rate constants observed under the same conditions for human NCBD.
251
252
253 **Discussion**
254
255 The biophysics and molecular evolution of NCBD is interesting for several reasons,
256 which all relate to the dynamic properties of NCBD. Firstly, while it has a hydrophobic
257 core and globular shape, NCBD is a very dynamic protein domain with characteristics
258 of an IDP (*5*, *6*, *8–11*, *25*). Secondly, NCBD has several binding partners including the
259 three NCOA transcriptional co-regulator paralogs (*5*, *26*), the transcription factors p53
260 (*27*), Ets-2 (*28*) and interferon factor-3 (*29*), and viral proteins such as Tax (*30*) from
261 T-cell leukemia virus. Intriguingly, NCBD displays great conformational plasticity as
262 shown by its complex with interferon factor-3 where the helices of NCBD adopt a
263 distinct conformation as compared to the complex with CID (*31*). Thirdly, evolutionary

264 snapshots of the complex between CID and NCBD suggest that several new
265 intermolecular contacts and conformational plasticity increased the affinity when going
266 from the Cambrian-like $NCBD_{D/P}^{ML}$ (K_d ~ 1-5 μM) to younger variants (K_d ~ 0.2 μM)
267 (*12*, *13*, *32*). Fourthly, while affinity and structural order of modern NCBD/CID
268 complexes were increased, the transition state of the folding-induced binding displayed
269 more conformational heterogeneity as compared to the ancestral complex (*33*). Our
270 present results, how the free, unbound state of NCBD has evolved during the transition
271 from a low-affinity to a high-affinity CID binder relate to all four points.
272
273 The most striking finding is that $NCBD_{D/P}^{ML}$ displays very similar molten-globule like
274 properties as the previously characterized human NCBD (*8*, *10*). This conservation of
275 properties, borderline between a globular domain and an IDP, suggests that the
276 dynamics of NCBD is preserved by purifying selection and therefore of functional
277 importance. In general, structural plasticity is regarded as one main functional feature
278 of IDPs allowing for multiple protein-protein interactions (*34*). NCBD interacts with
279 several protein domains, both folded and disordered ones, and the dynamic nature of
280 NCBD likely increases its propensity to adapt to different partners. Moreover, NCBD
281 interactions result in coupled folding and binding. Many such reactions have recently
282 been shown to occur via a mechanism denoted templated folding, where the binding
283 partner influences the folding pathway (*35–37*). Indeed, this was observed for the
284 interaction between human NCBD and CID (*33*, *38*, *39*). Thus, our present findings
285 suggest that templated folding may be a general feature of binding reactions with
286 NCBD where the conserved dynamics facilitate sampling of different free states,
287 heterogeneity of bound states, as well as the pathway between free and bound states.
288

289 Going into details of the NMR model, we note that while overall structure is robust to
290 errors in the predicted sequence as shown by the comparison of the NMR models of
291 free $NCBD_{D/P}^{ML}$ and $NCBD_{D/P}^{AltAll}$, there are differences in for example helix
292 orientations. Globular domains with a sequence identity as high as these NCBD variants
293 (77-88%) would typically have identical structures due to a highly funneled energy
294 landscape (*40*, *41*), while proteins with larger structural heterogeneity have less
295 funneled landscapes (*1*). Indeed, the differences between the structures of $NCBD_{Human}$,
296 $NCBD_{D/P}^{ML}$ and $NCBD_{D/P}^{AltAll}$, in particular regarding the angles of the helices in
297 relation to each other, are consistent with a less funneled energy landscape resulting in
298 conformational heterogeneity (*11*). This heterogeneity is also consistent with the
299 conserved dynamic properties of NCBD. In conclusion, our data suggest evolutionarily
300 conserved dynamics of NCBD that underlie functional plasticity in ground state
301 conformations, templated binding-and-folding and a propensity to interact with several
302 binding partners.
303
304
305 **Materials and methods**
306
307 **Protein sequences, expression and purification.** The reconstruction of ancestral
308 sequences was previously published (*12*). The AltAll versions of $NCBD_{D/P}$ (Fig. 1) and
309 CID_{1R} used in the present paper was based on posterior probabilities from the
310 reconstruction with a cutoff of 91%. One position in $NCBD_{D/P}$ (Thr2062) is very
311 uncertain. A Thr residue (15%) was originally chosen at this position in $NCBD_{D/P}^{ML}$ to
312 avoid a hydrophobic residue, although Ile (19%) has a higher posterior probability. In
313 the current $NCBD_{D/P}^{AltAll}$ residue 2062 is Ile. NCBD and CID variants were expressed

314 in *E. coli* from a pRSETA plasmid and purified as previously described (*33*)
315 Concentrations were determined by absorbance at 280 nm for NCBD (using calculated
316 extinction coefficients based on amino acid composition) or 205 nm for CID using an
317 extinction coefficient of 250,000 $M^{-1}cm^{-1}$. Purity was checked by SDS-PAGE and
318 identity of the purified proteins was confirmed by MALDI-TOF mass spectrometry.
319
320 **Circular dichroism**. Far-UV CD experiments were performed using a JASCO J-1500
321 CD spectrophotometer with a Peltier temperature control system. The protein
322 concentration in all CD experiments was 18-20 μM. The buffer solution was either 20
323 mM sodium phosphate (pH 7.4), 150 mM NaCl or 50 mM potassium formate (pH 3.0),
324 150 mM NaCl, and CD spectra were recorded at 277 K. The scanning speed was 50
325 nm/min, bandpass 1 nm and integration time 1 second. Each reported spectrum is an
326 average of 3-4 recorded spectra. In the equilibrium thermal denaturation experiments
327 the proteins were dissolved in 50 mM potassium formate buffer (pH 3.0), 150 mM NaCl
328 and the sample was heated from 277 to 368 K. The heating rate was 1 K/min, waiting
329 time 5 seconds and the denaturation was monitored at 222 nm. During the heating,
330 spectra (average of three measurements) were taken at 283, 303, 323, 343 and 363 K,
331 respectively. In the equilibrium urea denaturation experiments the proteins were
332 denatured in 0-6.6 M urea at 277 K and the unfolding was monitored at 222 nm. The
333 data was analyzed in GraphPad Prism and fitted by non-linear regression to a two-state
334 equilibrium model (*42*). Because of the broad unfolding transition and lack of native
335 baseline for several variants, four parameters were shared among all urea denaturation
336 data sets in the curve fitting (Fig. S4, Supplementary Table 1). One of these parameters
337 was the molar ellipticity of the native state, with the reasonable assumption that the
338 secondary structures of the native states are similar for all variants. The other

339 parameters were the slopes of the denatured and native baselines as well as the m_{D-N}
340 value (assuming a similar change in solvent accessible surface area upon denaturation
341 for all variants).
342
343 **Temperature jump experiments.** Temperature jump experiments were conducted
344 using 100-200 μM protein on a TJ-64 temperature jump system (TgK Scientific). The
345 buffer solution was 20 mM sodium phosphate (pH 7.4), 150 mM NaCl. The proteins
346 were subjected to temperature jumps of 2-8.5 K to different target temperatures. The
347 data were fitted in the Kinetic Studio software (TgK scientific) to a double exponential
348 function, to account both for the fast phase (relaxation time ~ 80 μs), which corresponds
349 to the heating time of the instrument, and to the slow phase, which corresponds to the
350 conformational transition in the protein. A Trp variant of $NCBD_{D/P}^{ML}$ ($NCBD_{D/P}^{T2073W}$)
351 was chosen for kinetic experiments since a Trp in this position was previously used for
352 human NCBD. We engineered a Trp at other positions in $NCBD_{D/P}^{ML}$ and obtained rate
353 constants in the same range for all variants (Supplementary Table S2).
354
355 **Stopped flow experiments.** The stopped flow experiments were performed using an
356 upgraded SX-17MV stopped flow spectrophotometer (Applied Photophysics) and the
357 measurements were conducted at 277 K. Proteins were dissolved in 5 mM HCl (pH ~
358 2) and rapidly mixed 1:1 with buffer solutions complemented with trimethylamine N-
359 oxide (TMAO) to a final concentration of 20 mM sodium phosphate (pH 7.4), 150 mM
360 NaCl, 1 M TMAO. The final protein concentration was 5 μM. The excitation
361 wavelength was 280 nm and the resulting fluorescence emission was detected after
362 passage through a 330 nm bandpass filter. The transients were analyzed in GraphPad
363 Prism and fitted to a single or double exponential function.

364

365 **NMR experiments**. NMR experiments were acquired on Bruker 600, 700 and 900
366 MHz spectrometers equipped with triple resonance cryogenic temperature probes at
367 298 K except otherwise stated. The final NMR samples contained 500 μM protein to
368 which 0.01% NaN_3 and 5% D_2O was added. Experiments for assignment and
369 subsequent structure determination were done at pH 2.4 (HCl adjusted with NaOH) for
370 $NCBD_{D/P}^{ML}$ and pH 6.8 for $NCBD_{D/P}^{AltAll}$. The following NMR experiments were
371 recorded for assignment and subsequent structure determination: standard 2D ^{1}H-^{15}N
372 HSQC, 3D HNCACB ^{15}N-resolved [^{1}H-^{1}H]-NOESY-HSQC, ^{15}N-TOCSY-HSQC ^{13}C-
373 resolved [^{1}H-^{1}H]-NOESY-HSQC, HCCH-TOCSY and ^{13}C-resolved [^{1}H-^{1}H]-TOCSY-
374 HSQC. Phi-angle restraining $^{3}J_{HNHA}$ couplings were determined from 3D HNHA type
375 experiments using quantitative -*J* intensity modulated experiments (*43*). The
376 temperature variation experiments were performed in 20 mM sodium formate, pH 3.0.
377 All experiments were processed with nmrpipe (*44*) and analysed with CCPnmr (*45*).

378

379 **Structure calculation**. Structure calculations were done using the CYANA 3.97 (*46*)
380 package as follows: Initially, cross peaks were converted into upper distance restraints
381 following an automated process in CYANA. These distance restraints together with
382 φ/ψ dihedral angles determined from C^{α}-chemical shifts and $^{3}J_{HNH}\alpha$ (measured) were
383 used as input for the initial structure calculations. The structures were calculated with
384 200,000 torsion angle dynamics steps for 100 conformers starting from random torsion
385 angles by simulated annealing. 20 conformers with the lowest target function values
386 were selected and analyzed. The structural statistics together with all input data for the
387 structure calculations are presented in Supplementary Table S3. Assignments and

structural coordinates have been deposited in the RCSB protein data bank with pdb code: 7OSR (accession number BMRB ID 34635) ($NCBD_{D/P}^{ML}$) and 7OSW (accession number BMRB ID 34636) ($NCBD_{D/P}^{AltAll}$).

Acknowledgements

This work was supported by the Wenner-Gren foundation WG-17 returning grants to C. N. C., and by the Swedish Research Council (2020-04395 to P.J.) and Knut and Alice Wallenberg foundation (Evolution of new genes and proteins, to P.J.). We used the NMR Uppsala infrastructure, which is funded by the Department of Chemistry - BMC and the Disciplinary Domain of Medicine and Pharmacy. We thank Magnus Kjaergaard for valuable comments on the NMR experiments.

401

402 **References**

403 1. S. Gianni, M. I. Freiberger, P. Jemth, D. U. Ferreiro, P. G. Wolynes, M. Fuxreiter,
404 Fuzziness and Frustration in the Energy Landscape of Protein Folding, Function,
405 and Assembly. *Acc Chem Res*. **54**, 1251–1259 (2021).

406 2. O. F. Lange, N.-A. Lakomek, C. Farès, G. F. Schröder, K. F. A. Walter, S.
407 Becker, J. Meiler, H. Grubmüller, C. Griesinger, B. L. de Groot, Recognition
408 dynamics up to microseconds revealed from an RDC-derived ubiquitin ensemble
409 in solution. *Science*. **320**, 1471–1475 (2008).

410 3. S. J. Wodak, E. Paci, N. V. Dokholyan, I. N. Berezovsky, A. Horovitz, J. Li, V. J.
411 Hilser, I. Bahar, J. Karanicolas, G. Stock, P. Hamm, R. H. Stote, J. Eberhardt, Y.
412 Chebaro, A. Dejaegere, M. Cecchini, J.-P. Changeux, P. G. Bolhuis, J. Vreede,
413 P. Faccioli, S. Orioli, R. Ravasio, L. Yan, C. Brito, M. Wyart, P. Gkeka, I.
414 Rivalta, G. Palermo, J. A. McCammon, J. Panecka-Hofman, R. C. Wade, A. Di
415 Pizio, M. Y. Niv, R. Nussinov, C.-J. Tsai, H. Jang, D. Padhorny, D. Kozakov, T.
416 McLeish, Allostery in Its Many Disguises: From Theory to Applications.
417 *Structure*. **27**, 566–578 (2019).

418 4. H. J. Dyson, P. E. Wright, Role of Intrinsic Protein Disorder in the Function and
419 Interactions of the Transcriptional Coactivators CREB-binding Protein (CBP)
420 and p300. *J. Biol. Chem.* **291**, 6714–22 (2016).

421 5. C. H. Lin, B. J. Hare, G. Wagner, S. C. Harrison, T. Maniatis, E. Fraenkel, A
422 small domain of CBP/p300 binds diverse proteins: solution structure and
423 functional studies. *Mol Cell*. **8**, 581–590 (2001).

424 6. S. J. Demarest, M. Martinez-Yamout, J. Chung, H. Chen, W. Xu, H. J. Dyson, R.
425 M. Evans, P. E. Wright, Mutual synergistic folding in recruitment of CBP/p300
426 by p160 nuclear receptor coactivators. *Nature*. **415**, 549–553 (2002).

427 7. M.-O. Ebert, S.-H. Bae, H. J. Dyson, P. E. Wright, NMR relaxation study of the
428 complex formed between CBP and the activation domain of the nuclear hormone
429 receptor coactivator ACTR. *Biochemistry*. **47**, 1299–308 (2008).

430 8. M. Kjaergaard, K. Teilum, F. M. Poulsen, Conformational selection in the molten
431 globule state of the nuclear coactivator binding domain of CBP. *Proc. Natl.*
432 *Acad. Sci. U.S.A.* **107**, 12535–12540 (2010).

433 9. M. Kjaergaard, F. M. Poulsen, K. Teilum, Is a malleable protein necessarily
434 highly dynamic? The hydrophobic core of the nuclear coactivator binding
435 domain is well ordered. *Biophys J*. **102**, 1627–1635 (2012).

436 10. M. Kjaergaard, L. Andersen, L. D. Nielsen, K. Teilum, A folded excited state of
437 ligand-free nuclear coactivator binding domain (NCBD) underlies plasticity in
438 ligand recognition. *Biochemistry*. **52**, 1686–1693 (2013).

11. E. Papaleo, C. Camilloni, K. Teilum, M. Vendruscolo, K. Lindorff-Larsen, Molecular dynamics ensemble refinement of the heterogeneous native state of NCBD using chemical shifts and NOEs. *PeerJ*. **6**, e5125 (2018).

12. G. Hultqvist, E. Åberg, C. Camilloni, G. N. Sundell, E. Andersson, J. Dogan, C. N. Chi, M. Vendruscolo, P. Jemth, Emergence and evolution of an interaction between intrinsically disordered proteins. *Elife*. **6**, e16059 (2017).

13. P. Jemth, E. Karlsson, B. Vögeli, B. Guzovsky, E. Andersson, G. Hultqvist, J. Dogan, P. Güntert, R. Riek, C. N. Chi, Structure and dynamics conspire in the evolution of affinity between intrinsically disordered proteins. *Sci. Adv.* **4**, eaau4130 (2018).

14. G. N. Eick, J. T. Bridgham, D. P. Anderson, M. J. Harms, J. W. Thornton, Robustness of Reconstructed Ancestral Protein Functions to Statistical Uncertainty. *Mol Biol Evol*. msw223 (2016).

15. K. M. Hart, M. J. Harms, B. H. Schmidt, C. Elya, J. W. Thornton, S. Marqusee, Thermodynamic system drift in protein evolution. *PLoS Biol*. **12**, e1001994 (2014).

16. L. Laursen, J. Čalyševa, T. J. Gibson, P. Jemth, Divergent Evolution of a Protein-Protein Interaction Revealed through Ancestral Sequence Reconstruction and Resurrection. *Mol Biol Evol*. **38**, 152–167 (2021).

17. P. D. Williams, D. D. Pollock, B. P. Blackburne, R. A. Goldstein, Assessing the accuracy of ancestral protein reconstruction methods. *PLoS Comput Biol*. **2**, e69 (2006).

18. V. A. Risso, J. A. Gavira, E. A. Gaucher, J. M. Sanchez-Ruiz, Phenotypic comparisons of consensus variants versus laboratory resurrections of Precambrian proteins. *Proteins*. **82**, 887–896 (2014).

19. M. L. Romero-Romero, V. A. Risso, S. Martinez-Rodriguez, B. Ibarra-Molero, J. M. Sanchez-Ruiz, Engineering ancestral protein hyperstability. *Biochem J*. **473**, 3611–3620 (2016).

20. D. L. Trudeau, M. Kaltenbach, D. S. Tawfik, On the Potential Origins of the High Stability of Reconstructed Ancestral Proteins. *Mol Biol Evol*. **33**, 2633–2641 (2016).

21. L. C. Wheeler, S. A. Lim, S. Marqusee, M. J. Harms, The thermostability and specificity of ancient proteins. *Curr Opin Struct Biol*. **38**, 37–43 (2016).

22. T. W. Hearing, T. H. P. Harvey, M. Williams, M. J. Leng, A. L. Lamb, P. R. Wilby, S. E. Gabbott, A. Pohl, Y. Donnadieu, An early Cambrian greenhouse climate. *Sci Adv*. **4**, eaar5690 (2018).

23. T. Wotte, C. B. Skovsted, M. J. Whitehouse, A. Kouchinsky, Isotopic evidence for temperate oceans during the Cambrian Explosion. *Sci Rep*. **9**, 6330 (2019).

24. J. Dogan, A. Toto, E. Andersson, S. Gianni, P. Jemth, Activation Barrier-Limited Folding and Conformational Sampling of a Dynamic Protein Domain. *Biochemistry*. **55**, 5289–5295 (2016).

25. S. J. Demarest, S. Deechongkit, H. J. Dyson, R. M. Evans, P. E. Wright, Packing, specificity, and mutability at the binding interface between the p160 coactivator and CREB-binding protein. *Protein Sci.* **13**, 203–210 (2004).

26. J. Xu, Q. Li, Review of the in vivo functions of the p160 steroid receptor coactivator family. *Mol. Endocrinol.* **17**, 1681–1692 (2003).

27. J. A. Livengood, K. E. S. Scoggin, K. Van Orden, S. J. McBryant, R. S. Edayathumangalam, P. J. Laybourn, J. K. Nyborg, p53 Transcriptional activity is mediated through the SRC1-interacting domain of CBP/p300. *J Biol Chem*. **277**, 9054–9061 (2002).

28. G. Jayaraman, R. Srinivas, C. Duggan, E. Ferreira, S. Swaminathan, K. Somasundaram, J. Williams, C. Hauser, M. Kurkinen, R. Dhar, S. Weitzman, G. Buttice, B. Thimmapaya, p300/cAMP-responsive element-binding protein interactions with ets-1 and ets-2 in the transcriptional activation of the human stromelysin promoter. *J Biol Chem*. **274**, 17342–17352 (1999).

29. S. Matsuda, J. C. Harries, M. Viskaduraki, P. J. F. Troke, K. B. Kindle, C. Ryan, D. M. Heery, A Conserved alpha-helical motif mediates the binding of diverse nuclear proteins to the SRC1 interaction domain of CBP. *J Biol Chem*. **279**, 14055–14064 (2004).

30. K. E. Scoggin, A. Ulloa, J. K. Nyborg, The oncoprotein Tax binds the SRC-1-interacting domain of CBP/p300 to mediate transcriptional activation. *Mol Cell Biol*. **21**, 5520–5530 (2001).

31. B. Y. Qin, C. Liu, H. Srinath, S. S. Lam, J. J. Correia, R. Derynck, K. Lin, Crystal structure of IRF-3 in complex with CBP. *Structure*. **13**, 1269–1277 (2005).

32. E. Karlsson, A. Lindberg, E. Andersson, P. Jemth, High affinity between CREBBP/p300 and NCOA evolved in vertebrates. *Protein Sci.* **29**, 1687–1691 (2020).

33. E. Karlsson, C. Paissoni, A. M. Erkelens, Z. A. Tehranizadeh, F. A. Sorgenfrei, E. Andersson, W. Ye, C. Camilloni, P. Jemth, Mapping the transition state for a binding reaction between ancient intrinsically disordered proteins. *J Biol Chem*. **295**, 17698–17712 (2020).

34. P. E. Wright, H. J. Dyson, Intrinsically disordered proteins in cellular signalling and regulation. *Nat Rev Mol Cell Biol*. **16**, 18–29 (2015).

35. A. Toto, C. Camilloni, R. Giri, M. Brunori, M. Vendruscolo, S. Gianni, T. A, C. C, G. R, B. M, V. M, G. S., Molecular Recognition by Templated Folding of an Intrinsically Disordered Protein. *Sci. Rep.* **6**, 21994 (2016).

36. A. Toto, F. Malagrinò, L. Visconti, F. Troilo, L. Pagano, M. Brunori, P. Jemth, S. Gianni, Templated folding of intrinsically disordered proteins. *J. Biol. Chem.* **295**, 6586–6593 (2020).

37. D. Wu, H.-X. Zhou, W. D, Z. HX., Designed Mutations Alter the Binding Pathways of an Intrinsically Disordered Protein. *Sci. Rep.* **9**, 6172 (2019).

38. P. Jemth, X. Mu, Å. Engström, J. Dogan, A frustrated binding interface for intrinsically disordered proteins. *J. Biol. Chem.* **289**, 5528–5533 (2014).

39. E. Karlsson, E. Andersson, J. Dogan, S. Gianni, P. Jemth, C. Camilloni, A structurally heterogeneous transition state underlies coupled binding and folding of disordered proteins. *J. Biol. Chem.* **294**, 1230–1239 (2019).

40. C. Chothia, A. M. Lesk, The relation between the divergence of sequence and structure in proteins. *EMBO J.* **5**, 823–826 (1986).

41. M. Oliveberg, P. G. Wolynes, The experimental survey of protein-folding energy landscapes. *Q. Rev. Biophys.* **38**, 245–288 (2005).

42. A. Fersht, *Structure and mechanism in protein science: a guide to enzyme catalysis and protein folding.* (Macmillan, 1999).

43. N.-A. Lakomek, J. Ying, A. Bax, Measurement of ^{15}N relaxation rates in perdeuterated proteins by TROSY-based methods. *J Biomol NMR*. **53**, 209–221 (2012).

44. F. Delaglio, S. Grzesiek, G. W. Vuister, G. Zhu, J. Pfeifer, A. Bax, NMRPipe: a multidimensional spectral processing system based on UNIX pipes. *J Biomol NMR*. **6**, 277–293 (1995).

45. W. F. Vranken, W. Boucher, T. J. Stevens, R. H. Fogh, A. Pajon, M. Llinas, E. L. Ulrich, J. L. Markley, J. Ionides, E. D. Laue, The CCPN data model for NMR spectroscopy: development of a software pipeline. *Proteins*. **59**, 687–696 (2005).

46. P. Güntert, C. Mumenthaler, K. Wüthrich, Torsion angle dynamics for NMR structure calculation with the new program Dyana. *J. Mol. Biol.* **273**, 283–298 (1997).

545 **Figures**

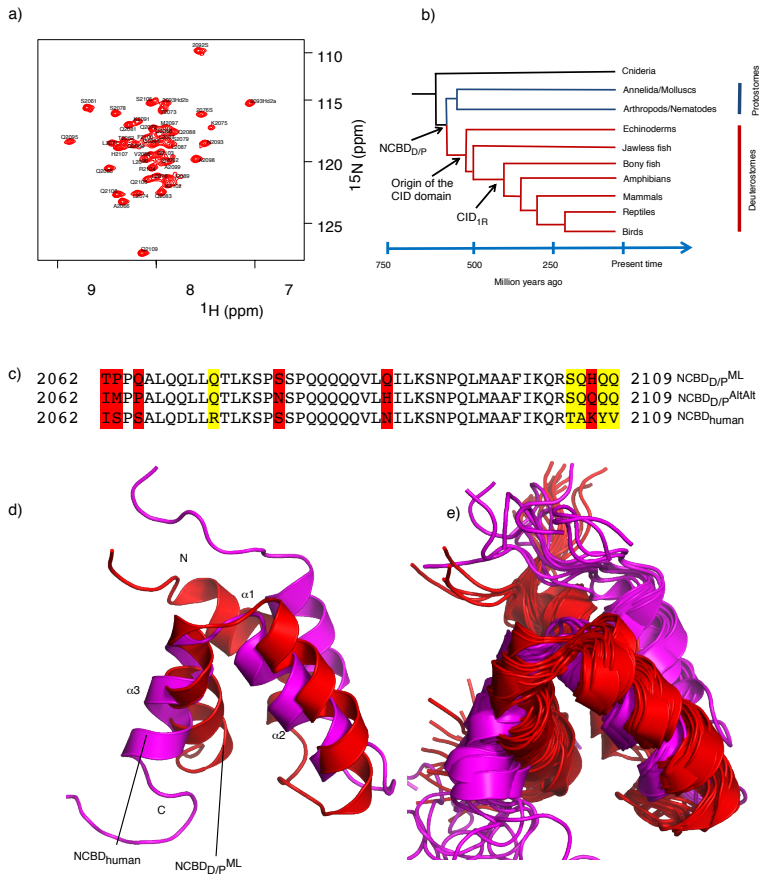

546

547 **Figure 1. Structures of ancestral and human NCBD domains**. (a) ^{1}H-^{15}N HSQC
548 spectrum of $NCBD_{D/P}^{ML}$ at pH 2.4 with assigned residues. All assignments and the
549 structural coordinates have been deposited in the pdb data bank with accession
550 number BMRB ID 34635 and pdb code: 7OSR. (b) A schematic tree depicting the
551 relationship between the deuterostome/protostome (D/P) ancestor and modern
552 species. The times on the x-axis are approximate, in particular the divergence of
553 protostomes and deuterostomes. (c) Sequence alignment for $NCBD_{Human}$, $NCBD_{D/P}^{ML}$
554 $NCBD_{D/P}^{AltAlt}$. The residues differing between $NCBD_{D/P}^{ML}$ and $NCBD_{D/P}^{AltAlt}$ are
555 marked in red while additional differences to $NCBD_{Human}$ are marked in yellow. (d)
556 Comparison of the NMR structure of ancestral $NCBD_{D/P}^{ML}$ solved at low pH (red, pdb
557 code: 7OSR), and the previously determined human NCBD (magenta, 2KKJ) (*8*).

Note that the structure of human NCBD was solved using a slightly longer construct.

(e) Overlay of the 20 lowest energy structures of the $NCBD_{D/P}^{ML}$ domain with those of $NCBD_{human}$.

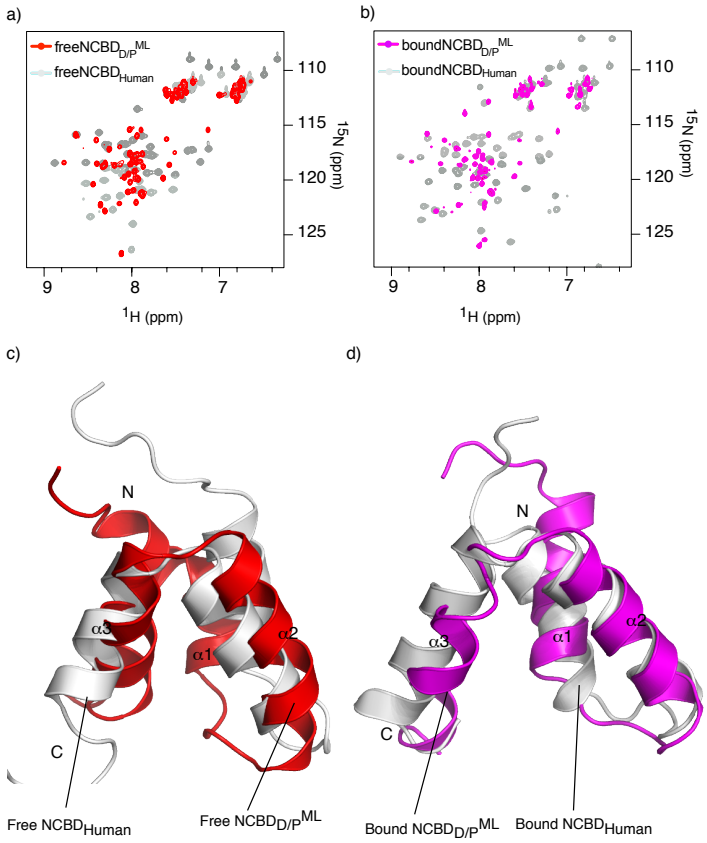

Figure 2. Comparison of the ligand-free and bound ancestral NCBD$_{D/P}^{ML}$ and extant NCBD$_{Human}$. The ligand-bound conformations (pdb codes 6ES5 and 6ES7) and the structure of free human NCBD (pdb code: 2KKJ) (*8*) were previously determined. (a) Overlay of the ^{1}H-^{15}N HSQC spectra between free NCBD$_{D/P}^{ML}$ (red) and free NCBD$_{Human}$ (grey). (b) Overlay of the ^{1}H-^{15}N HSQC spectra between CID-bound NCBD$_{D/P}^{ML}$ (magenta) and CID-bound NCBD$_{Human}$ (grey). Structural alignment between (c) free NCBD$_{D/P}^{ML}$ (red, 7OSR) and free NCBD$_{Human}$ (grey, 2KKJ), and (d) CID-bound NCBD$_{D/P}^{ML}$ (magenta, , 6ES5) and CID-bound NCBD$_{Human}$ (grey, 6ES7).

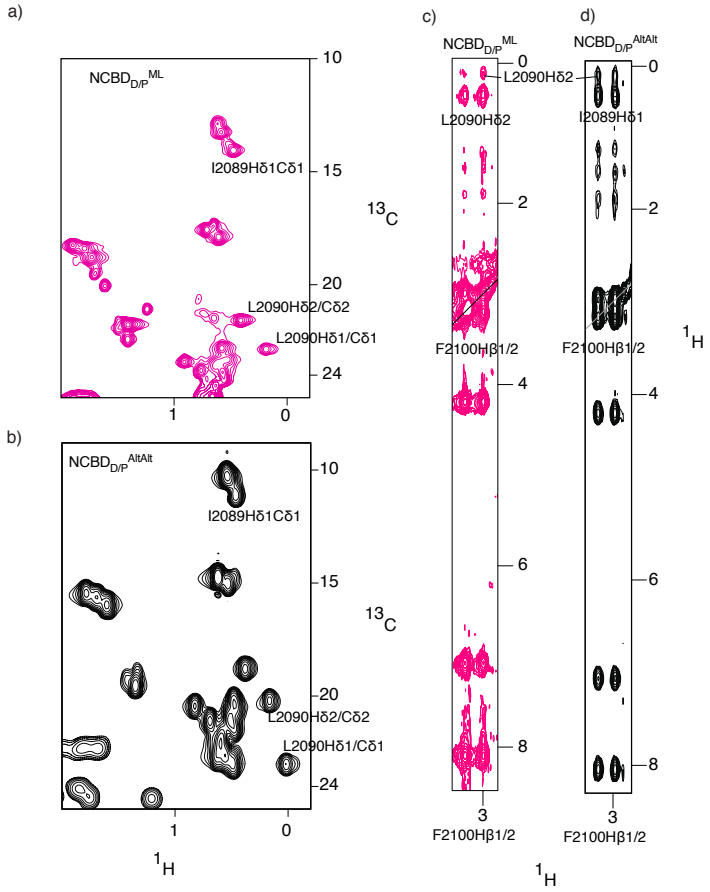

572

573 **Figure 3. Phe2100 makes NOEs to Ile2089 and Leu2090 in NCBD$_{D/P}^{ML}$ and**
574 **NCBD$_{D/P}^{AltAlt}$.** (a) ^{1}H-^{13}C HSQC spectra of the methyl region of NCBD$_{D/P}^{ML}$, showing
575 the Hδ1-Cδ1 shifts of L2090 and I2089. (b) ^{1}H-^{13}C HSQC spectra of the methyl region
576 of NCBD$_{D/P}^{AltAlt}$, showing the Hδ1-Cδ1 shifts of L2090 and I2089. (c) Strip from a ^{1}H-
577 ^{1}H ^{13}C resolved NOESY showing NOEs from the Hβ1/2 atoms of Phe2100 and the
578 associated NOEs to Leu2090Hδ1 for NCBD$_{D/P}^{ML}$. (d) Strip from a ^{1}H-^{1}H ^{13}C resolved
579 NOESY showing NOEs from the Hβ1/2 atoms of Phe2100 and the associated NOEs to
580 Leu2090Hδ1 and Ile2089Hδ1 for NCBD$_{D/P}^{AltAlt}$. These signature NOEs implies that
581 both proteins form a hydrophobic core similar to that of NCBD$_{Human}$.

582

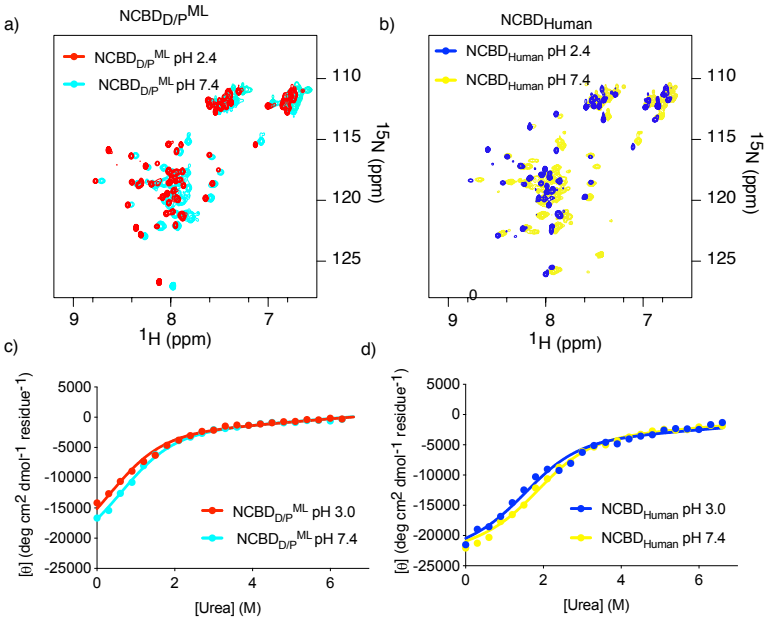

Figure 4. Comparison of ancestral NCBD$_{D/P}^{ML}$ and extant NCBD$_{Human}$ at two different pH values. a) Overlay of the ^{1}H-^{15}N HSQC spectra of NCBD$_{D/P}^{ML}$ at pH 2.4 (red) and at pH 6.8 (cyan). b) Overlay of the ^{1}H-^{15}N HSQC spectra of NCBD$_{Human}$ at pH 2.4 (blue) and at pH 6.8 (yellow). c) Urea denaturation experiments for NCBD$_{D/P}^{ML}$ at pH 3.0 (red) and at pH 7.4 (cyan). d) Urea denaturation experiments for NCBD$_{Human}$ at pH 3.0 (yellow) and at pH 7.4 (blue).

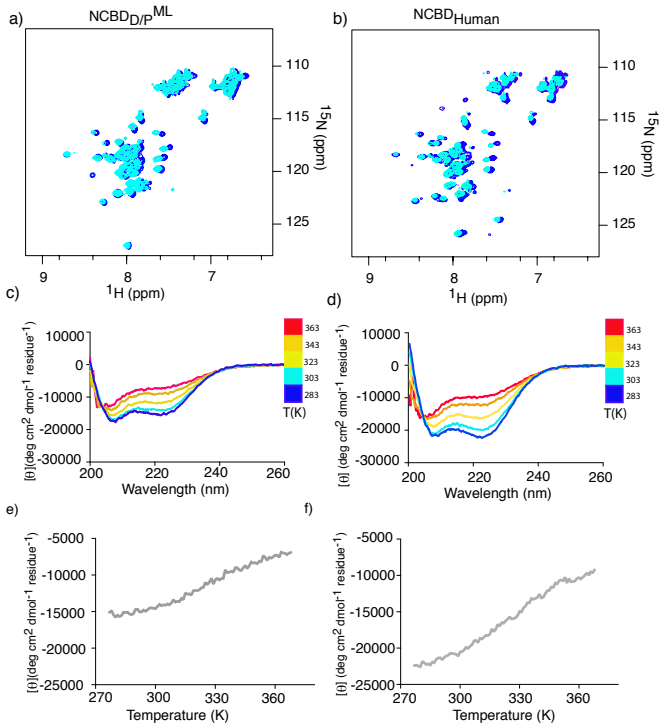

591

592 **Figure 5. Temperature dependence for ancestral NCBD$_{D/P}^{ML}$ and extant human**

593 **NCBD.** a) Overlay of ^{1}H-^{15}N HSQC spectra of NCBD$_{D/P}^{ML}$ at 283 K (blue) and at 303

594 K (cyan). b) Overlay of ^{1}H-^{15}N HSQC spectra of NCBD$_{Human}$ at 283 K (blue) and at 303

595 K (cyan). Circular dichroism spectra at a range of temperatures (283-363 K) for (c)

596 NCBD$_{D/P}^{ML}$ and (d) NCBD$_{Human}$. Molecular ellipticity at 222 nm (probing α-helix

597 content) as a function of temperature for (e) NCBD$_{D/P}^{ML}$ and (f) NCBD$_{Human}$.

598

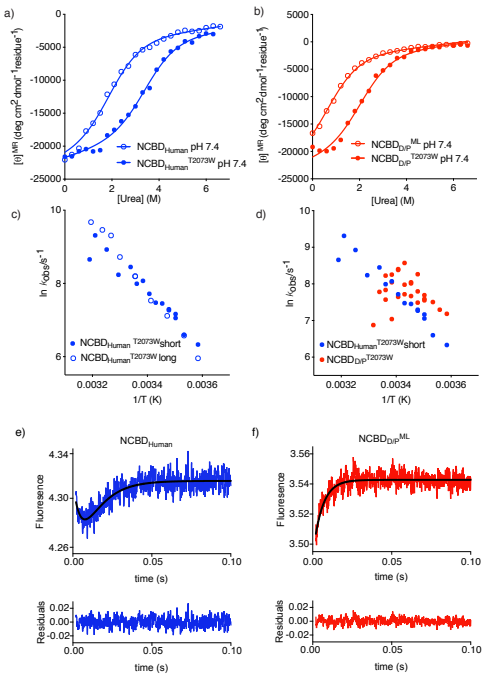

Figure 6. Stability and temperature dependence of kinetic rate constants for NCBD$_{D/P}^{ML}$ and extant human NCBD. (a) Stability measurement of NCBD$_{Human}^{WT}$ (open circles) and NCBD$_{Human}^{T2073W}$ (filled circles) measured by urea denaturation. (b) Stability measurement of NCBD$_{D/P}^{ML}$ (open circles) and NCBD$_{D/P}^{T2073W}$ (filled circles). Parameters from the curve fitting are shown in Supplementary Table S1. (c) Temperature jump kinetic experiments for a longer human NCBD construct used in previous studies (*24*) (open circles) and the shorter human NCBD variant used in this study (filled circles). Both variants contained the T2073W mutation. (d) A comparison of observed rate constants from temperature-jump experiments for NCBD$_{Human}^{T2073W}$ (blue) and NCBD$_{D/P}^{T2073W}$ (red). All experiments were performed in 20 mM sodium phosphate pH 7.4, 150 mM NaCl. (e-f) Kinetic (un)folding of NCBD$_{Human}^{T2073W}$ and NCBD$_{D/P}^{T2073W}$ measured by stopped flow fluorescence spectroscopy. (e) (Un)folding kinetic transient of NCBD$_{Human}^{T2073W}$ (blue) fitted to a double exponential function (black line). Below each transient are the residuals from the respective fits. (f) Stopped flow (un)folding kinetic transient of NCBD$_{D/P}^{T2073W}$

615 (red) fitted to a single exponential function (black line). The experiments were

616 performed by jumping from 5 mM HCl (pH ~ 2) to a final buffer concentration of 20

617 mM sodium phosphate (pH 7.4), 150 mM NaCl, 1 M TMAO. The relaxation was

618 monitored using a 330 band-pass emission filter. Fitting a double exponential function

619 resulted in k_{obs} values of 290 ± 30 and 67 ± 4 s^{-1} for $NCBD_{Human}^{T2073W}$. Fitting a single

620 exponential function yielded a k_{obs} value of 139 ± 7 s^{-1} for $NCBD_{D/P}^{T2073W}$.

621

622

Supplementary information

The dynamic properties of a nuclear coactivator binding domain are evolutionarily conserved

Elin Karlsson[1], Frieda A. Sorgenfrei[1,†], Eva Andersson[1], Jakob Dogan[1], Per Jemth[1,*], and Celestine N. Chi[1,2,*]

[1]Department of Medical Biochemistry and Microbiology, Uppsala University, BMC Box 582, SE-75123 Uppsala, Sweden.

[2]Department of Pharmaceutical Biosciences, Uppsala University, BMC Box 582, SE-75123 Uppsala, Sweden

[†]Present address: acib GmbH, Krenngasse 37, 8010 Graz c/o University of Graz, Institute of Chemistry, NAWI Graz, BioTechMed Graz, Heinrichstrasse 28, 8010 Graz, Austria

*Correspondence to

Celestine Chi, Celestine.Chi@imbim.uu.se

Per Jemth, Per.Jemth@imbim.uu.se

Supplementary figures

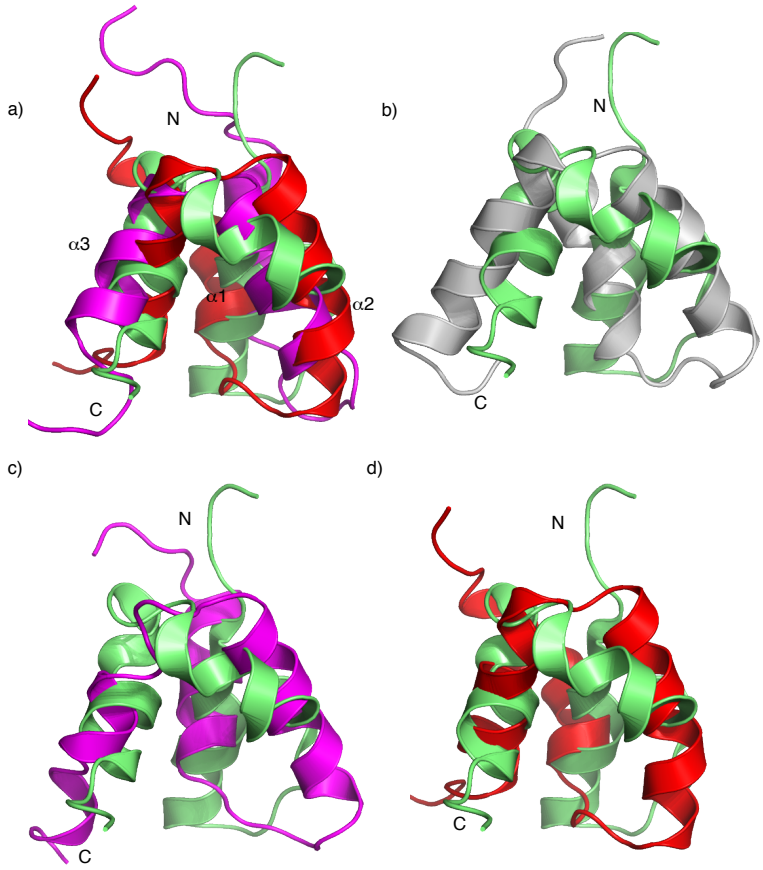

Figure S1. Overlay of the structures of $NCBD_{D/P}^{ML}$, $NCBD_{D/P}^{AltAlt}$ and $NCBD_{Human}$. (a) An overlay of the structures determined from NMR for $NCBD_{D/P}^{ML}$(red, pdb code: 7OSR), $NCBD_{D/P}^{AltAlt}$ (green, 7OSW), and the previously determined $NCBD_{Human}$ (magenta, 2KKJ). (b) Overlay of $NCBD_{D/P}^{AltAlt}$ (green, 7OSW), and the previously determined CID-bound $NCBD_{D/P}^{ML}$ (grey, 6ES5). (c) Overlay of $NCBD_{D/P}^{AltAlt}$ (green, 7OSW), and the previously determined $NCBD_{Human}$ (magenta, 2KKJ). (d) Overlay of $NCBD_{D/P}^{AltAlt}$ (green, 7OSW) and $NCBD_{D/P}^{ML}$ (red, 7OSR).

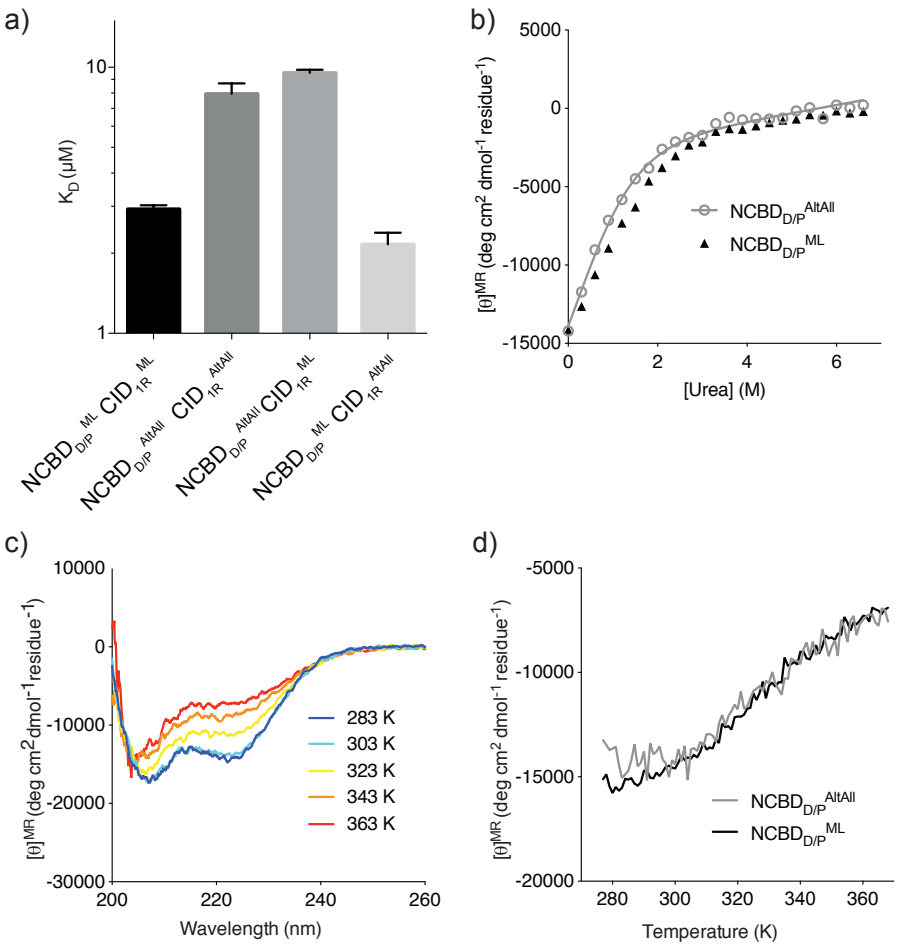

Figure S2. The biophysical properties of NCBD$_{D/P}^{ML}$ are robust to errors in the sequence. a) Binding affinities of NCBD$_{D/P}^{ML}$ or NCBD$_{D/P}^{AltAlt}$ and CID$_{1R}^{ML}$ or CID$_{1R}^{AltAll}$ measured with ITC. The buffer solution was 20 mM sodium phosphate pH 7.4, 150 mM NaCl. (b) Stability of NCBD$_{D/P}^{AltAll}$ measured by urea denaturation in 50 mM formate (pH 3.0), 150 mM NaCl. The CD signal at 222 nm was monitored and the data was fitted to a two-state function. A reliable [urea]$_{50\%}$ value could not be obtained, although qualitative comparison with NCBD$_{D/P}^{ML}$ indicates that the stability of the two variants is similar. (c-d) Temperature stability for NCBD$_{D/P}^{AltAll}$. The CD signal at 222 nm was monitored and spectra were taken at temperatures 283-363 K.

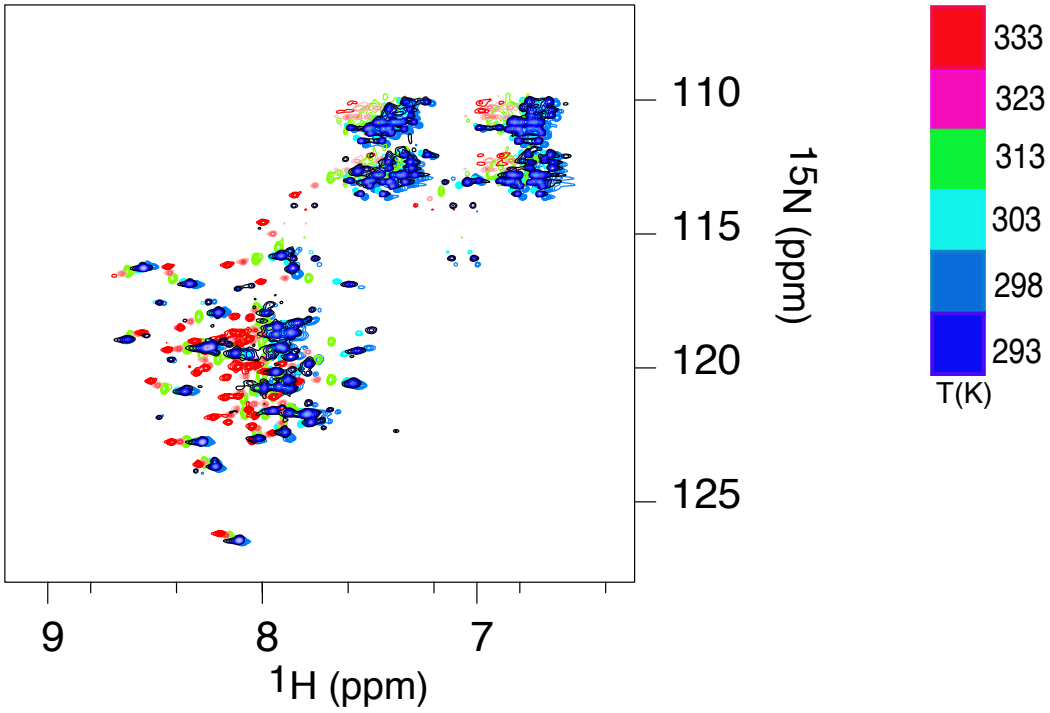

Figure S3. ^{15}N-^{1}H HSQC spectra of NCBD$_{D/P}^{ML}$ at different temperatures. The experiments were performed from 293 K (blue) to 333 K (red).

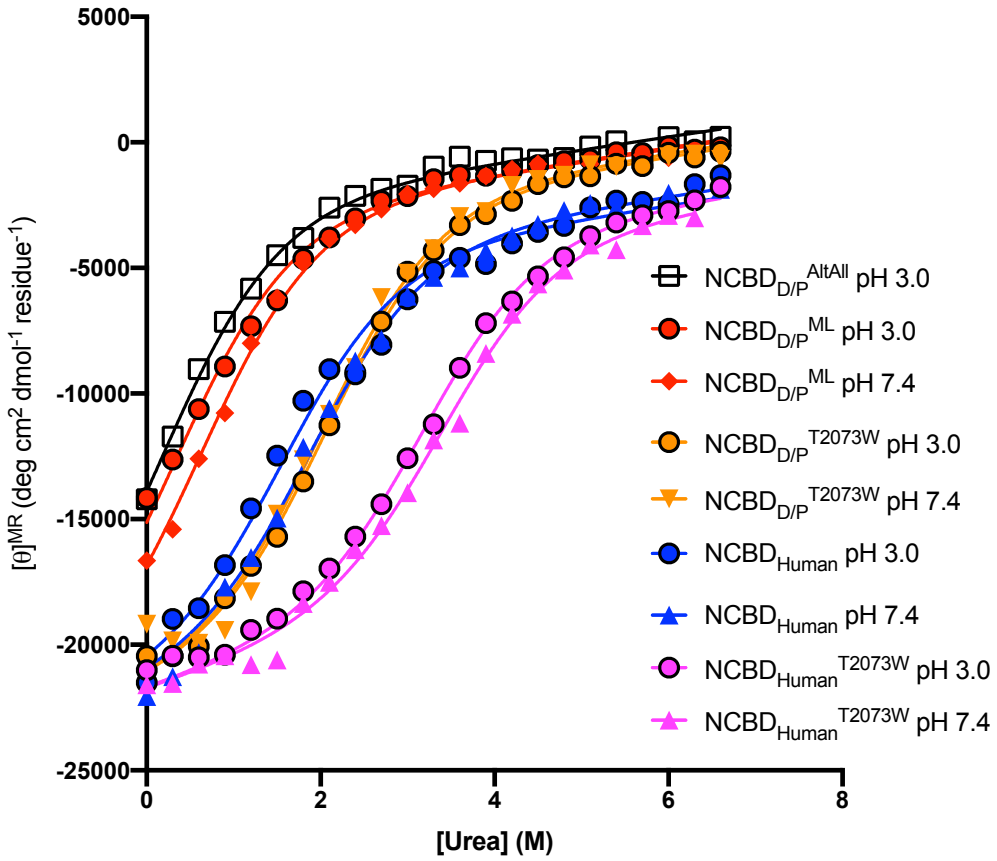

Figure S4. Equilibrium urea denaturation experiments. All data sets were fitted simultaneously to a two-state model in GraphPad Prism with shared parameters for the native state molar ellipticity, the denatured and native baseline slopes and the $m_{D\text{-}N}$ value. Experiments were performed in either 50 mM potassium formate buffer (pH 3.0), 150 mM NaCl or 20 mM sodium phosphate buffer (pH 7.4), 150 mM NaCl. The shared $m_{D\text{-}N}$ value was fitted as 0.74 ± 0.07 kcal $mol^{-1}M^{-1}$.

Supplementary Tables

Supplementary Table S1. Stabilities of NCBD variants expressed as the urea concentration at 50% denaturation. The proteins were denatured with urea and the structural transition was monitored with CD at 222 nm at 277 K. The solutions were either 50 mM potassium formate buffer (pH 3.0), 150 mM NaCl or 20 mM sodium phosphate buffer (pH 7.4), 150 mM NaCl. The data were fitted to a two-state model in GraphPad Prism. The parameters for the signal of the native state, the denatured and native baseline slopes, and the $m_{D\text{-}N}$ value were shared among the data sets in the curve fitting to allow fitting of the low stability $NCBD_{D/P}^{ML}$ and $NCBD_{D/P}^{AltAll}$ variants. The shared $m_{D\text{-}N}$ value was fitted as 0.82 ± 0.025 kcal $mol^{-1}M^{-1}$. The errors are the standard error from the curve fitting and likely a low estimate of.

Variant	**pH**	**$[Urea]_{50\%}$ (M)**	**$\Delta G_{D\text{-}N}$ (kcal/mol)**
$NCBD_{D/P}^{AltAll}$	3.0	0.22 ± 0.04	0.18 ± 0.03
$NCBD_{D/P}^{ML}$	3.0	0.38 ± 0.04	0.31 ± 0.03
$NCBD_{D/P}^{ML}$	7.4	0.68 ± 0.04	0.55 ± 0.04
$NCBD_{D/P}^{T2073W}$	3.0	2.13 ± 0.04	1.73 ± 0.06
$NCBD_{D/P}^{T2073W}$	7.4	2.08 ± 0.04	1.70 ± 0.06
$NCBD_{Human}$	3.0	1.61 ± 0.04	1.31 ± 0.05
$NCBD_{Human}$	7.4	1.94 ± 0.05	1.58 ± 0.06
$NCBD_{Human}^{T2073W}$	3.0	3.24 ± 0.07	2.64 ± 0.10
$NCBD_{Human}^{T2073W}$	7.4	3.46 ± 0.08	2.82 ± 0.11

Supplementary Table 2. Rate constants and kinetic amplitudes of folding for different D/P NCBD Trp variants measured in temperature jump experiments. The experiments were conducted using 200 μM protein in 20 mM sodium phosphate (pH 7.4), 150 mM NaCl. The jump in temperature was from 277 to 285.5 K.

Variant	**Amplitude**	k_{obs} **(s^{-1})**
$NCBD_{D/P}^{T2073W}$	1.06 ± 0.06	2400 ± 200
$NCBD_{D/P}^{L2067W}$	0.91 ± 0.02	1530 ± 50
$NCBD_{D/P}^{S2078W}$	0.35 ± 0.01	700 ± 60
$NCBD_{D/P}^{H2107W}$	0.47 ± 0.02	820 ± 80
$NCBD_{D/P}^{Q2108W}$	0.73 ± 0.02	960 ± 60

Supplementary Table 3

	$NCBD_{D/P}^{ML}$	$NCBD_{D/P}^{AltAlt}$
NMR distance and dihedral restraints		
Distance restraints		
Total NOEs	329	347
Intra-residue	113	145
Sequential ($\|i-j\| = 1$)	122	111
Medium-range ($1 < \|i-j\| < 4$)	76	76
Long-range ($\|i-j\| > 5$)	18	39
Total dihedral angle restraints	76	63
$^{3}J_{HN\alpha}$ scalar couplings	39	43
$^{13}C^{\alpha}$ chemical shifts	100	100
Structure statistics		
Average CYANA target function value ($Å^2$)	2.5 ± 0.2	2.8 ± 0.3
Violations		
Distance constraints (>0.5 Å)	0	0
Dihedral angle constraints (>5°)	0	0
Deviations from idealized geometry		
Bond lengths (Å)	0	0
Bond angles (°)	0	0
Impropers (°)	0	0
Average pairwise r.m.s. deviation (Å)		
Backbone residues	2.2 ± 1.0	0.5 ± 0.2
Heavy atoms residues	2.7 ± 1.0	1.0 ± 0.3